Contrib Mineral Petrol (2010) 160:261–277
DOI 10.1007/s00410-009-0476-4

ORIGINAL PAPER

Melt/rock interaction in remains of refertilized Archean lithospheric mantle in Jiaodong Peninsula, North China Craton: Li isotopic evidence

Hong-Fu Zhang · Etienne Deloule · Yan-Jie Tang · Ji-Feng Ying

Received: 21 July 2009 / Accepted: 26 November 2009 / Published online: 19 December 2009

Abstract Li contents and its isotopes of minerals in mantle peridotite xenoliths from late Cretaceous mafic dikes, analyzed in situ by Cameca IMS-1280, reveal the existence of melt/rock interaction in remains of refertilized Archean lithospheric mantle in Qingdao, Jiaodong Peninsula, North China Craton. Two groups of peridotites exist, i.e., low-Mg# lherzolite and high-Mg# harzburgites. The low-Mg# lherzolite has a relatively homogeneous Li concentration (ol: 2.01–2.11 ppm; opx: 1.77–1.88 ppm; cpx: 1.75–1.93 ppm) and Li isotopic composition (δ^7Li in ol: 4.2–7.6‰; in opx: 6.0–8.3‰; in cpx: 5.3–8.4‰). The similarity in δ^7Li value to the fresh MORB provides further evidence for the argument that the low-Mg# lherzolite could be the fragment of the newly accreted lithospheric mantle. The high-Mg# harzburgites have heterogeneous Li abundances (ol: 0.83–2.09 ppm; opx: 0.92–1.94 ppm; cpx: 1.12–4.89 ppm) and Li isotopic compositions (δ^7Li in ol: −0.5 to +11.5‰; in opx: −6.2 to +11.1‰; in cpx: −34.3 to +10.1‰), showing strong disequilibrium in Li partitioning and Li isotope fractionation between samples. The cores of most minerals in these high-Mg# harzburgites have relatively homogeneous δ^7Li values, which are higher than those of fresh MORB, but similar to those previously reported for arc lavas. These harzburgites have enriched trace elemental and Sr–Nd isotopic compositions. These observations indicate that in the early Mesozoic the lithospheric mantle beneath the southeastern North China Craton was similar to that in arc settings, which is metasomatized by subducted crustal materials. Extremely low δ^7Li preserved in cpxs requires diffusive fractionation of Li isotopes from later-stage melt into the minerals. Thus, the Li data provide further evidence that the Archean refractory lithospheric mantle represented by the high-Mg# harzburgites was refertilized through melt/rock interaction and transformed to the Mesozoic less refractory and incompatible element and Sr–Nd isotopes enriched lithospheric mantle.

Keywords Mantle xenoliths · Li content · Li isotope · Melt/rock interaction · Lithospheric mantle · North China Craton

Communicated by T. L. Grove.

Electronic supplementary material The online version of this article (doi:10.1007/s00410-009-0476-4) contains supplementary material, which is available to authorized users.

H.-F. Zhang (✉) · Y.-J. Tang · J.-F. Ying
State Key Laboratory of Lithospheric Evolution, Institute of Geology and Geophysics, Chinese Academy of Sciences, P.O. Box 9825, 100029 Beijing, China
e-mail: hfzhang@mail.igcas.ac.cn

E. Deloule
Centre National de la Recherche Scientifique, CRPG, BP20, 54501 Vandoeuvre-Les-Nancy Cedex, France

Introduction

Mineralogical and petrological investigations of Paleozoic kimberlite and Cenozoic basalt-borne mantle xenoliths and xenocrysts have revealed that the lithosphere of the North China Craton was not only considerably thinned, but also compositionally changed from Paleozoic-age cold and refractory lithospheric mantle to Cenozoic-age hotter and fertile mantle (Menzies et al. 2007 and references therein). Recent Re–Os analyses of Paleozoic kimberlite-borne mantle xenoliths and xenocrysts have demonstrated that both the garnet- and spinel-facies lithospheric mantle formed in the Archean (Gao et al. 2002; Wu et al. 2006;

Zhang et al. 2008a), thus the Archean lithospheric mantle indeed existed in the North China Craton prior to its thinning. However, the Re–Os isotopic systematics of the Cenozoic basalt-borne mantle xenoliths throughout the craton show that none of these xenoliths have Archean T_{RD} ages after its thinning (Zhang et al. 2009a and references therein). The overwhelming Proterozoic T_{RD} ages and their correlation with olivine Fo imply that the Archean lithospheric mantle was comprehensively refertilized by multiple-stage melt/rock interaction. Unfortunately, the composition and origin of the melts still remains unsolved.

To solve this problem, mantle xenoliths from the Mesozoic basalts should be a key. Recent studies on mantle peridotitic xenoliths from late Cretaceous basaltic rocks in Junan and Qingdao regions, Jiaodong Peninsula, have demonstrated the presence of two groups of mantle xenoliths: high-Mg# peridotites and low-Mg# peridotites (Ying et al. 2006; Zhang et al. 2009b). Although the low-Mg# peridotites could be the fragments of the late Meosozoic newly accreted lithospheric mantle after its thinning, the high-Mg# peridotites were indeed the remains of ancient lithospheric mantle (Ying et al. 2006; Zhang et al. 2009b). However, this ancient lithospheric mantle was also considerably refertilized by mantle metasomatism. Clinopyroxene (cpx) trace element and Sr–Nd isotopic data indicate that the diverse melts, perhaps partially from the continental crust, affected these high-Mg# xenoliths. To further investigate the composition and origin of the metasomatic melts, we use in situ Li concentrations and its isotopes of those peridotitic xenoliths that major and trace element compositions have already been well-constrained.

Lithium, a light alkali metal and mobile element, tends to partition preferentially into the melt/fluid phase during partial melting and melt/rock interaction (Brenan et al. 1998), leading to lithium enrichment in differentiated crust relative to the primitive mantle. Such a feature makes lithium and its isotopes a good geochemical tracer for many geological processes (Tang et al. 2007a and references therein), such as peridotite–melt interaction (Seitz and Woodland 2000; Seitz et al. 2004; Woodland et al. 2004; Jeffcoate et al. 2007; Wagner and Deloule 2007; Rudnick and Ionov 2007). Wagner and Deloule (2007), Rudnick and Ionov (2007) and Tang et al. (2007b) found large lithium elemental and isotopic disequilibria between minerals of peridotitic xenoliths from France, Russia and China, which were considered to be products of recent melt/fluid-rock reaction. The in situ analyses have shown that this lithium elemental and isotopic disequilibrium even exists within an individual mineral grains (Tang et al. 2007b; Wagner and Deloule 2007). The Li elemental and isotopic zonations observed in the minerals from the Hannuoba peridotitic xenoliths required that the melts derived from subducted altered oceanic crust were involved in the peridotite–melt interaction in the ancient lithospheric mantle. Thus, the Li abundance and its isotopes can provide important information for above geological events. In this paper, we selected five well-studied spinel-facies peridotites from Qingdao, Jiaodong Peninsula, for in situ Li elemental and its isotopic analyses, with aims (1) to clarify the abundance and distribution of lithium in mantle minerals, the intra- and inter-mineral fractionation of Li isotopes during melt/rock interaction; (2) to find the similarity or difference in Li abundances and its isotopes between the high-Mg# and low-Mg# group xenoliths and (3) to evaluate the composition and origin of the metasomatic melts involved in the modification of the ancient lithospheric mantle.

Xenolith petrology

The geological background of the Jiaodong Peninsula and the xenolith-host petrology and geochemistry of the Qingdao mafic dikes which intruded at *ca* 82 ± 4 Ma were described elsewhere in details (Zhang et al. 2008b, 2009b). Here, we just focus on the peridotitic xenolith petrology. All the peridotitic xenoliths investigated are spinel-facies nodules and include high-Mg# harzburgites and low-Mg# lherzolites. High-Mg# peridotites have inequigranular texture and high Fo olivines and high Cr# spinels. Cpxs in high-Mg# peridotites are generally LREE-enriched with variable REE concentrations (ΣREE = 5.6–85 ppm) and have enriched Sr–Nd isotopic compositions ($^{87}Sr/^{86}Sr = 0.7046–0.7087$; $^{143}Nd/^{144}Nd = 0.5121–0.5126$). These high-Mg# peridotites are considered to be fragments of ancient lithospheric mantle, which has experienced extensive interaction with diverse melts in Mesozoic time (Zhang et al. 2009b). The low-Mg# peridotites are equigranular and typified by low Fo in olivines and low Cr# in spinels. Cpxs from low-Mg# peridotites have low REE abundances, LREE-depleted REE patterns and depleted Sr–Nd isotopic feature, distinctive from the high-Mg# peridotites. These geochemical characteristics suggest that low-Mg# peridotites represent samples from the newly accreted lithospheric mantle. One low-Mg# lherzolite and four high-Mg# harzburgites, which were all well-characterized by both major and trace elemental geochemistry, were selected for Li content and Li isotopic study. One of high-Mg# harzburgites (PSK03-43) shows clear Fe-rich magma injection as shown by the aggregation of secondary spinels (Afig. 2a in electronic supplementary material).

Analytical methods

Li abundances and its isotopic compositions were determined with the Cameca IMS-1280 ion microprobe at the SIMS Lab, Institute of Geology and Geophysics, Chinese Academy of Sciences. The thin-section samples were gold-coated. A 13-kV, 10–20 nA O-primary beam was projected on an area of 20 μm in diameter. Positive secondary ions accelerated through 10 kV were measured at medium mass resolution ($M/\Delta M \sim 1{,}100$), with a transmitted field of 125 μm and an aperture field of 4,000, an energy window of 60 eV without energy offset. Primary beam position, entrance slits, contrast aperture, magnetic field and energy offset were automatically centered before each measurement. Secondary ions were counted on mono-collection pulse counting mode. Thirty to fifty cycles were measured with counting time of 12, 4 and 4 s for ^{6}Li, background at the 6.5 mass, and ^{7}Li, respectively. The counting rate on ^{7}Li ranges from 30,000 to 100,000 cps, depending on the sample Li content and primary beam intensity. A 60-s pre-sputtering without raster was applied before analysis. Li isotopic ratios are given in delta units using the δ^{7}Li notation $\{\delta^{7}\mathrm{Li} = [(^{7}\mathrm{Li}/^{6}\mathrm{Li}_{\mathrm{sample}})/(^{7}\mathrm{Li}/^{6}\mathrm{Li}_{\mathrm{LSVEC}}) - 1] \times 1{,}000$, with $^{7}\mathrm{Li}/^{6}\mathrm{Li}_{\mathrm{LSVEC}} = 12.0192$, Flesh et al. 1973}. Cpx BZ226 and BZ CG, Ol BZ29 and Opx BZ226 (Decitre et al. 2001) were used as standards (Fig. 1). Our measured values for these standards are -4.1 ± 0.7‰, $+10.9 \pm 0.6$‰, $+4.6 \pm 0.4$‰ and $+4.2 \pm 1.0$‰, respectively, consistent with the recommended values (−4.1‰, +10.5‰, +4.4‰ and +4.2‰, respectively) with analytical error. The 2σ errors for each measured point, including counting statistic and standard reproducibility, range from 1.5 to 2.5‰, depending on the mineral Li contents. The external 2σ on standard and some of the samples is lower than 1‰.

Note that the measured minerals in our samples display no major chemical variation at the mineral scale and a very limited range of chemical composition for the whole set, with high Mg# numbers (88–92) (Table 1) similar to the standard ones. This is what we expect for Li isotope analysis. The Li content and isotopic results are given in Table 1. The mineral Mg# numbers and cpx LREE/HREE fractionation as well as total REE abundances are also provided for comparison (data from Zhang et al. 2009b).

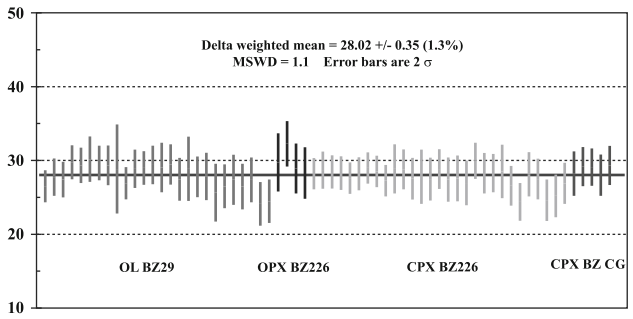

Fig. 1 Standard Li isotopic variation throughout the analyses with 2σ error bars

Analytical results

Low-Mg# peridotite

Li abundances

Olivine in the low-Mg# lherzolite shows a homogeneous Li abundance within and between crystals (2.01–2.11 ppm with an average of 2.06 ppm) (Table 1, Fig. 2; Afig. 1 in electronic supplementary material). Pyroxenes also have relatively constant Li abundances (opx: 1.77–1.88 ppm with an average of 1.81 ppm; cpx: 1.75–1.93 ppm with an average of 1.81 ppm) between individual grains although small intra-grain variation has been observed, especially in CPX 1, in which the core has slightly higher Li abundance than the rim (Table 1; Fig. 2; Afig. 1 in electronic supplementary material). Seitz and Woodland (2000) established a general Li partitioning relationship in an equilibrated peridotite in spinel-facies mantle: ol > cpx ≥ opx > > sp. This low-Mg# lherzolite is consistent with this ordering, showing Li equilibration in different mineral phases, but different from the Hannuoba spinel lherzolites which shows an enrichment of lithium in cpx relative to that in olivine (Tang et al. 2007b).

Li isotopes

Olivine in the low-Mg# lherzolite displays a narrow range of δ^{7}Li (4.2–7.6‰ with an average of 5.4‰), showing a relatively homogeneous Li isotope distribution between individual grains (Table 1; Fig. 2; Afig. 1 in electronic supplementary material), although an intra-grain zoning of δ^{7}Li exists in OL 1 with the core being slightly higher δ^{7}Li than one rim that has high Li concentration. Pyroxenes also have a narrow range of δ^{7}Li (opx: 6.0–8.3‰ with an average of 7.6 ± 1.48‰; cpx: 5.3–8.4‰ with an average of 6.9 ± 1.82‰) between different grains. A small intra-mineral zoning of δ^{7}Li has also been observed both in opx and cpx, in which the core of opx such as OPX 2 has slightly higher δ^{7}Li than the rim (Table 1; Fig. 2; Afig. 1 in electronic supplementary material), different from the feature of cpx which the core has lower δ^{7}Li than the rim. It should be noted that whereas the Li isotope zoning indeed exists in olivine and pyroxenes, the intra-mineral variation of δ^{7}Li is within the analytical uncertainty. All these δ^{7}Li values of minerals from Qingdao low-Mg#

Table 1 In situ analytical data on minerals of Qingdao peridotite xenoliths by Cameca IMS-1280

Mineral	Point	Li (ppm)	δ^7Li (‰)	2σ
PSK03-1212: Low-Mg# lherzolite, OL Fo = 89, OPX Mg# = 90, CPX Mg# = 91, $(La/Yb)_N$ = 0.3, ΣREE = 12 ppm				
OL1	1	2.03	4.8	1.4
	2	2.04	5.3	1.7
	3	2.04	5.5	1.5
	4	2.03	5.5	1.4
	5	2.08	4.6	1.5
	6	2.04	4.2	1.5
OL2	1	2.01	4.5	1.4
	2	2.08	7.6	1.4
OL3	1	2.11	5.2	1.2
	2	2.08	5.9	1.3
	3	2.06	5.6	1.2
	4	2.10	5.7	1.2
	5	2.04	5.6	1.2
	6	2.06	5.9	1.3
	7	2.05	4.6	1.2
OL4	1	2.05	5.1	1.2
	2	2.07	7.0	1.2
	3	2.04	5.9	1.2
	4	2.05	4.2	1.1
OPX1	1	1.77	7.6	1.5
	2	1.81	7.2	1.5
	3	1.88	7.1	1.4
	4	1.81	7.8	1.5
	5	1.78	7.9	1.5
	6	1.79	7.7	1.5
OPX2	1	1.79	7.4	1.5
	2	1.82	7.6	1.5
	3	1.79	8.3	1.5
	4	1.77	8.3	1.5
	5	1.80	7.8	1.4
	6	1.88	6.0	1.5
CPX1	1	1.79	7.6	2.3
	2	1.83	5.4	2.0
	3	1.93	6.3	1.8
	4	1.87	6.9	1.7
	5	1.81	8.1	1.7
CPX2	1	1.75	8.4	1.7
	2	1.77	7.1	1.7
	3	1.78	5.3	1.8
	4	1.75	7.3	1.7
PSK03-43: High-Mg# harzburgite, OL Fo = 91, OPX Mg# = 91.3, CPX Mg# = 91.7, $(La/Yb)_N$ = 15, ΣREE = 85 ppm				
OL1	1	1.68	5.2	1.4
	2	1.69	4.8	1.3
	3	1.67	5.3	1.3
	4	1.67	4.1	1.2

Table 1 continued

Mineral	Point	Li (ppm)	δ^7Li (‰)	2σ
OL2	1	1.66	4.5	1.2
	2	1.67	5.0	1.2
	3	1.69	4.6	1.3
	4	1.69	5.1	1.3
	5	1.66	4.7	1.2
	6	1.69	4.7	1.2
	7	1.72	4.6	1.2
OPX1	1	0.92	6.6	1.9
	2	0.93	8.4	1.9
	3	1.17	3.7	2.1
OPX2	1	1.26	6.1	1.6
	2	1.31	6.8	1.6
	3	1.27	7.8	1.6
	4	1.23	10.3	1.6
	5	1.28	9.1	1.6
OPX3	1	1.28	6.9	1.6
	2	1.28	7.2	1.6
	3	1.25	8.6	1.8
CPX1	1	1.47	−4.0	1.7
	2	1.34	6.9	1.8
	3	1.37	2.9	1.8
CPX2	1	0.00	−18.5	38.6
CPX3	1	1.29	9.6	1.9
	2	1.26	9.1	2.1
	3	2.06	0.3	1.8
PSK03-48: High-Mg# harzburgite, OL Fo = 91, OPX Mg# = 91.5, CPX Mg# = 91.6, $(La/Yb)_N$ = 14.7, ΣREE = 82 ppm				
OL1	1	0.96	6.6	1.7
	2	0.96	10.7	1.7
	3	0.92	10.8	1.8
	4	0.97	10.5	1.7
	5	0.89	11.5	2.1
	6	2.09	−0.5	2.5
OL2	1	0.94	9.3	1.6
	2	0.94	9.4	1.6
	3	0.92	10.1	2.0
OPX1	1	1.35	5.0	1.6
	2	1.31	8.0	1.7
	3	1.27	11.1	1.7
	4	1.42	7.7	2.0
	5	1.32	8.2	1.8
	6	1.31	6.5	1.7
	7	1.35	5.9	1.6
	8	1.34	5.2	1.7

Table 1 continued

Mineral	Point	Li (ppm)	δ^7Li (‰)	2σ
CPX1	1	1.77	10.1	1.7
	2	1.72	9.2	1.7
	3	1.70	10.0	1.9
	4	1.71	8.2	1.7
	5	1.70	9.7	1.7
	6	1.92	6.7	1.8
CPX2	1	1.30	9.8	2.2
	2	2.00	6.0	1.9
	3	1.25	7.7	1.9
PSK03-410: High-Mg# harzburgite, OL Fo = 91, OPX Mg# = 91.5, CPX Mg# = 91.6, $(La/Yb)_N$ = 36, ΣREE = 33 ppm				
OL1	1	0.83	6.6	2.5
	2	0.83	7.7	2.5
	3	0.84	5.1	2.9
OL2	1	1.02	6.7	2.1
	2	1.02	7.3	2.0
	3	1.00	6.2	2.0
OPX1	1	1.93	−0.9	1.4
	2	1.94	−1.2	1.3
	3	1.93	−0.9	1.4
CPX1	1	1.54	7.5	2.4
	2	1.63	3.5	2.3
	3	2.52	−17.0	2.5
CPX2	1	1.56	7.6	2.4
	2	1.69	−15.7	2.3
	3	3.16	−30.6	1.4
	4	2.08	−34.3	1.7
PSK03-414: High-Mg# harzburgite, OL Fo = 91.5, OPX Mg# = 92, CPX Mg# = 93, $(La/Yb)_N$ = 2.9, ΣREE = 5.6 ppm				
OL1	1	1.59	2.8	1.4
	2	1.57	1.7	1.4
	3	1.56	2.7	1.4
	4	1.75	3.1	1.3
OL2	1	1.58	2.1	1.3
	2	1.53	1.3	1.3
	3	1.65	2.3	1.4
OL3	1	1.62	0.9	1.3
	2	1.64	2.4	1.3
	3	1.58	1.3	1.3
	4	1.60	2.1	1.3
OPX1	1	1.07	5.7	1.8
	2	1.25	−6.2	1.6
	3	1.02	8.3	1.8
	4	1.06	3.7	2.0
OPX2	1	1.03	5.3	1.9
	2	1.00	7.6	2.0
	3	1.03	5.0	2.0
CPX1	1	1.12	6.9	2.0
	2	1.22	2.1	2.4

Table 1 continued

Mineral	Point	Li (ppm)	δ^7Li (‰)	2σ
CPX2	1	4.89	8.8	8.3
	2	1.66	−1.9	1.7
	3	1.68	−0.3	1.7
	4	2.34	−13.9	1.5

Major and trace element data are taken from Zhang et al. (2009b). Mg# = Mg/(Mg + Fe) × 100. $(La/Yb)_N$ is chondrite-normalized La/Yb ratio. Normalization values are from Anders and Grevesse (1989)

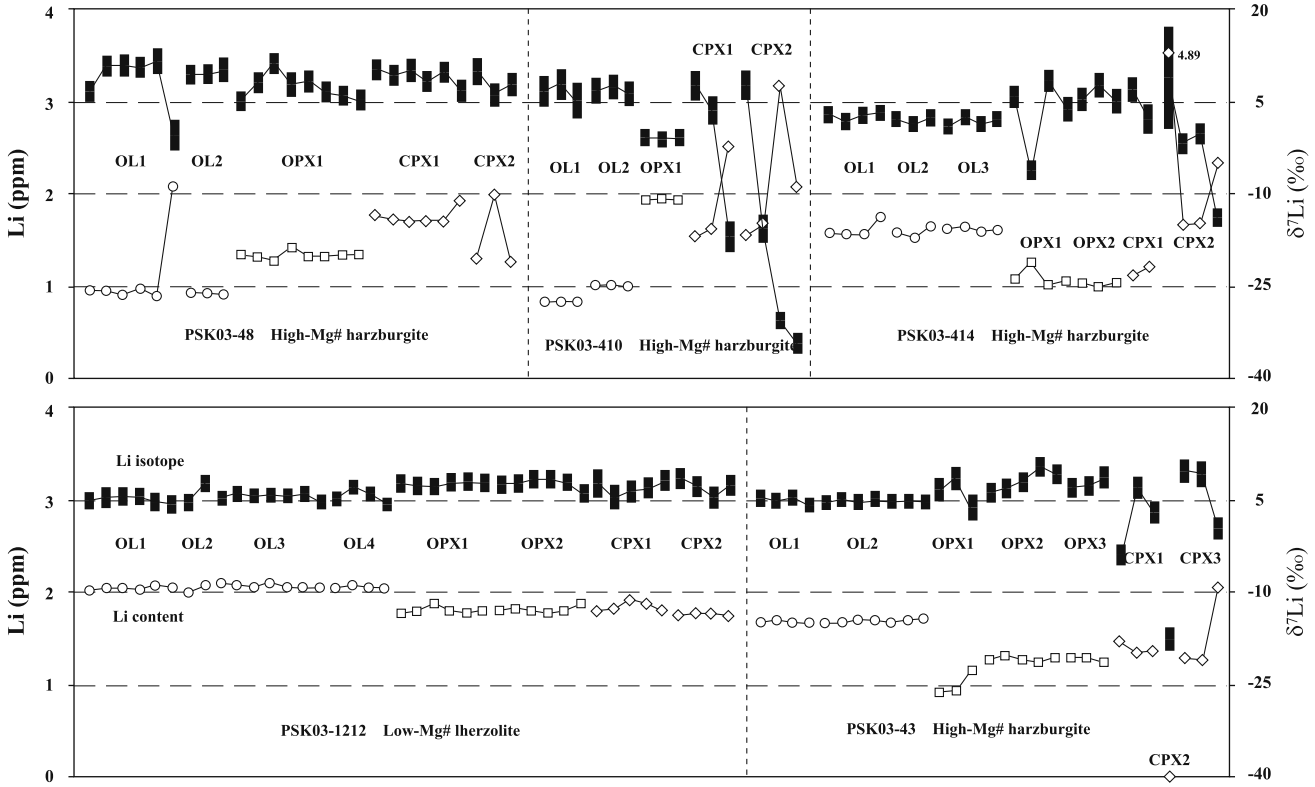

Fig. 2 Li content and Li isotopic variation between and within minerals in Qingdao peridotitic xenoliths

xenolith fall within the field for the fresh MORB (Fig. 3; Tomascak et al. 2008).

High-Mg# peridotites

Li abundances

Large and clear variations in Li abundances have been observed between samples and mineral phases, even within minerals, in the high-Mg# harzburgite xenoliths (Table 1, Fig. 2; Afig. 2–5 in electronic supplementary material). However, different minerals have different features. Olivines have relatively homogeneous Li abundances within and between individual grains, but show some variations between samples (PSK03-43: 1.66–1.72 ppm; PSK03-48: 0.89–0.97 ppm with one rim up to 2.09 ppm; PSK03-410: 0.83–1.02 ppm; PSK03-414: 1.53–1.75 ppm). Olivine Li abundances in high-Mg# harzburgites thus are lower than those in low-Mg# lherzolite, with only one rim possessing the Li content identical to olivine in low-Mg# lherzolite (Fig. 2). Similarly, orthopyroxene (opx) also has relatively homogeneous Li abundance within individual grain, but shows small variation between grains and samples (PSK03-43: 0.92–1.31 ppm; PSK03-48: 1.27–1.42 ppm; PSK03-410: 1.93–1.94 ppm; PSK03-414: 1.0–1.25 ppm). In contrast, cpxs have large variations in Li abundances between grains and samples, and are extremely heterogeneous

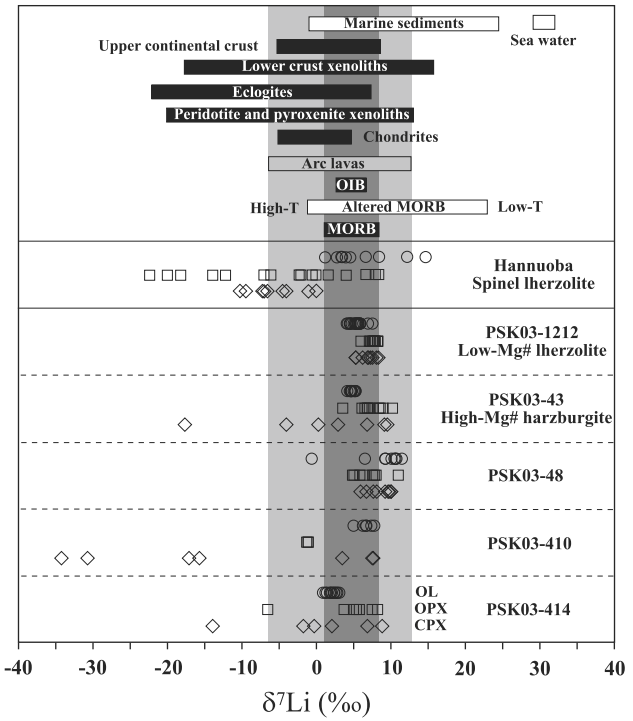

Fig. 3 Li isotope variations in minerals of Qingdao peridotitic xenoliths, in comparison with Hannuoba spinel lherzolites as well as various reservoirs. Data sources: Hannuoba spinel lherzolites (Tang et al. 2007b); Fresh and altered MORB (Chan et al. 1992; Moriguti and Nakamura 1998a; Tomascak et al. 2008); OIB or oceanic island basalts (Tomascak et al. 1999; Chan and Frey 2003; Chan et al. 2009); Chondrites and lower crust xenoliths (Tomascak 2004; Teng et al. 2008); Peridotite and pyroxenite xenoliths (Seitz and Woodland 2000; Nishio et al. 2004; Tomascak 2004; Brooker et al. 2004; Seitz et al. 2004; Woodland et al. 2004; Magna et al. 2006; Jeffcoate et al. 2007; Rudnick and Ionov 2007; Tang et al. 2007b; Wagner and Deloule 2007; Aulbach et al. 2008; Ionov and Seitz 2008; Aulbach and Rudnick 2009); Eclogites (Zack et al. 2003; Marschall et al. 2007); Arc lavas (Moriguti and Nakamura 1998a; Tomascak et al. 2000, 2002; Chan et al. 2002a, b; Agostini et al. 2008; Košler et al. 2009); Upper continental crust (Teng et al. 2004); Marine sediments (Chan et al. 1994; Zhang et al. 1998; James et al. 1999; Chan and Kastner 2000; Bouman et al. 2004); Sea water (Chan and Edmond 1988; You and Chan 1996; Moriguti and Nakamura 1998b; Tomascak et al. 1999)

within mineral grain (PSK03-43: 1.26–2.06 ppm; PSK03-48: 1.25–2.0 ppm; PSK03-410: 1.54–3.16 ppm; PSK03-414: 1.12–4.89 ppm). Thus, the cpxs have the highest Li abundances, followed by the opxs with the lowest Li abundances in olivines except for sample PSK03-414. This Li abundance ordering is different from the Seitz and Woodland (2000) equilibrated Li partitioning relationship, but similar to the ordering observed in Hannuoba spinel lherzolite xenoliths (Tang et al. 2007b) and the xenoliths suite studied by Rudnick and Ionov (2007), showing disequilibrium Li partitioning between mineral phases.

Li isotopes

Although the clear Li isotope zoning has been observed in some olivines and opxs with the cores being higher than the rims, the variations of δ^7Li in olivine and opx between different grains and samples are limited in high-Mg# harzburgites (Table 1, Fig. 2; Afig. 2–5 in electronic supplementary material) (the average δ^7Li_{ol} vs. δ^7Li_{opx} for PSK03-43: 4.8 ± 1.2 vs. 7.4 ± 1.7‰; PSK03-48: 8.7 ± 1.8 vs. 7.2 ± 1.7‰; PSK03-410: 6.6 ± 2.3 vs. -1.0 ± 1.4‰; PSK03-414: 2.1 ± 1.3 vs. 4.2 ± 1.9‰). The Li isotope fractionation of opx relative to olivine in PSK03-43 ($\Delta^7Li_{opx\text{-}ol} = \delta^7Li_{opx} - \delta^7Li_{ol} = 2.6$) and PSK03-414 ($\Delta^7Li_{opx\text{-}ol} = 2.1$) is compatible with that in low-Mg# lherzolite.

Clinopyroxene in high-Mg# harzburgites has an extremely large intra- and inter-grain variation of δ^7Li between samples (Table 1, Fig. 2; Afig. 2–5 in electronic supplementary material) (PSK03-43: $-4.0 \sim +9.6$‰; PSK03-48: $+6.0 \sim +10.1$‰; PSK03-410: $-34.3 \sim +7.6$‰; PSK03-414: $-13.9 \sim +8.8$‰), showing an exceedingly heterogeneous δ^7Li. Cpxs in sample PSK03-48 and some analyses in other samples have higher δ^7Li values than fresh MORB field, which are close to the δ^7Li values for co-existing opxs and olivines, falling in the arc lavas and altered MORB fields (Fig. 3). However, the predominant data for cpx δ^7Li are very low, such low δ^7Li values were recently observed in opxs of Hannuoba spinel lherzolites (Tang et al. 2007b), metasomatized peridotite and pyroxenite xenoliths (Brooker et al. 2004; Rudnick and Ionov 2007), eclogites (Zack et al. 2003), and lower crust xenoliths (Teng et al. 2008). Few analyses are even down to less than -30‰ (Table 1; Fig. 3). Li isotopes have a general negative correlation with Li abundance within and between samples (Fig. 4), i.e., the higher Li abundance in cpx the lower δ^7Li it has.

Discussion

Homogeneity of Li contents and Li isotopes in low-Mg# lherzolite

The narrow range of Li contents observed in individual mineral phases (Fig. 2) indicates that the low-Mg# lherzolite has an approximately equilibrated partitioning of lithium between different grains. Slightly higher Li content in olivine of this xenolith relative to co-existent pyroxenes follows the Li partitioning relationship in an equilibrated peridotite in spinel-facies mantle: ol > cpx ≥ opx, as established by Seitz and Woodland (2000) and newly obtained mineral/melt partition coefficients for Li (Ottolini et al. 2009). This indicates that the Li equilibrium had been

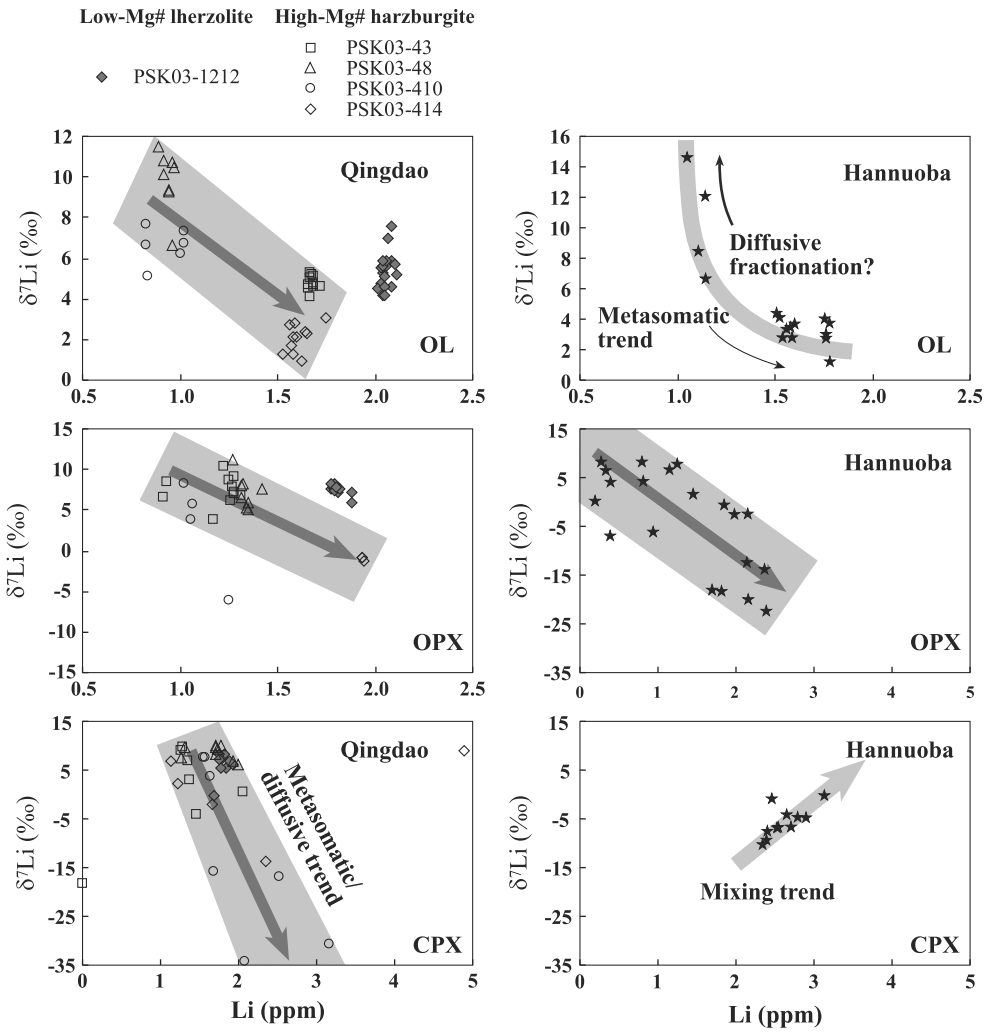

Fig. 4 Li content vs. Li isotope in minerals of Qingdao peridotitic xenoliths. The *star* shows the SIMS data from Hannuoba (Tang et al. 2007b)

almost achieved not only between individual grains but also between mineral phases. This conclusion is further supported by the plots of Li in cpx vs. Li in opx or ol (Fig. 5), in which the low-Mg# lherzolite plots within or close to the fields for equilibrium partitioning of mantle xenoliths. All these features imply that the Li distribution in the low-Mg# peridotite is almost at equilibrium.

The Li abundances in olivine and pyroxenes of low-Mg# lherzolite are slightly higher than those for normal mantle, i.e., fertile to moderately depleted peridotites (Woodland et al. 2004), and the bulk-rock Li content as calculated from mineral mode (1.97 ppm, $ol_{62}opx_{26}cpx_{12}$, Zhang et al. 2009b) is also close to the normal mantle. Lithium is a moderately incompatible element and prefers to partition into melt during mantle partial melting (Ottolini et al. 2009). The Li abundance close to the normal mantle reveals that the low-Mg# lherzolite only underwent a very low degree of partial melting, consistent with the result of melting calculation (5%) obtained from the trace element composition of cpx and with relative fertile major element compositions of minerals (Zhang et al. 2009b). The high Li depletion relative to other trace elements in cpx (Fig. 6) indicates that the Li prefers to partition into olivine in equilibrated mantle mineral phases, as compared with other trace elements, which mainly tend to stay in cpx.

The narrow δ^7Li range in individual minerals and the absence of a large variation between co-existent mineral phases ($\Delta^7Li_{opx\text{-}ol} = \delta^7Li_{opx} - \delta^7Li_{ol} = 2.2$; $\Delta^7Li_{cpx\text{-}ol} = \delta^7Li_{cpx} - \delta^7Li_{ol} = 1.5$) indicate that Li isotopic compositions between different phases approach equilibrium in the low-Mg# lherzolite, showing a relatively homogeneous Li isotope distribution (Fig. 2). These δ^7Li values for Qingdao low-Mg# lherzolite fall almost within the field for the fresh MORB (Fig. 3; Chan et al. 1992; Moriguti and Nakamura 1998a; Tomascak et al. 2008), which was believed to be derived from the partial melting of asthenosphere. Tomascak et al. (1999) found that Li isotopes do not show per mil-level mass fractionation at

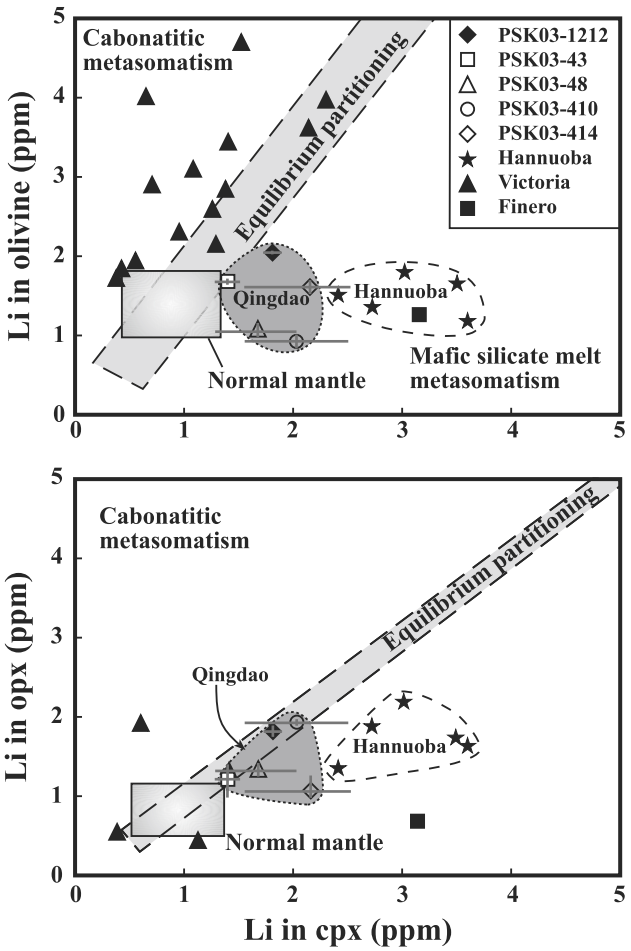

Fig. 5 Li–Li diagram showing Li abundances in coexisting cpx, opx and olivine (modified from Woodland et al. 2004). Li concentrations in normal mantle, i.e., fertile to moderately depleted peridotites, are from Seitz and Woodland (2000). The shadow field represents equilibrium partitioning. Data for Victoria and Finero samples are from Woodland et al. (2004) and Seitz and Woodland (2000), respectively. The TIMS data from Hannuoba are from Tang et al. (2007b). Mineral Li data from Qingdao xenoliths is the average of the individual sample, with *error bars* showing the range of predominant analyses

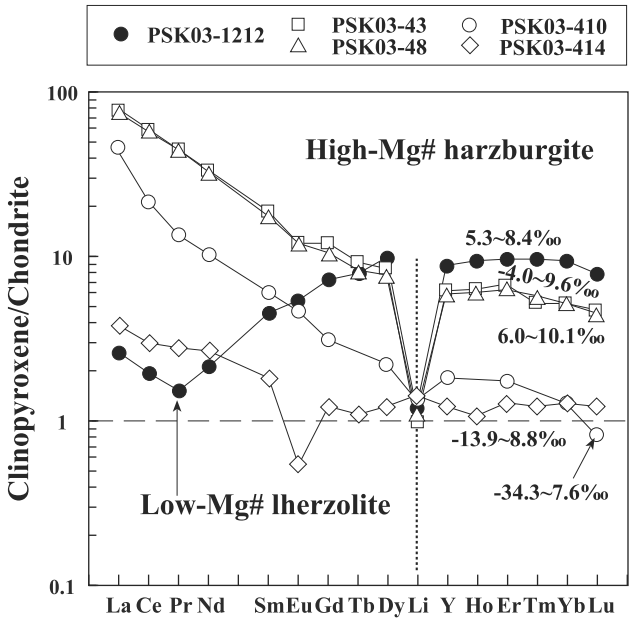

Fig. 6 Chondrite-normalized trace element diagram showing the Li depletion or enrichment relative to other trace elements. Chondrite-normalized value is from Anders and Grevesse (1989). Average trace element concentration in cpx is from Zhang et al. (2009b). Li abundance is the average result of the analyses. The range of δ^7Li in cpx is also shown on

temperatures of magmatic processes. This conclusion has been further supported by the constant isotopic values of bulk rocks and olivine separates from basaltic lavas (Chan and Frey 2003; Jeffcoate et al. 2007). Experimental results also indicate that Li isotopic fractionation between mantle minerals and fluid at temperatures over 900°C is < 1.0‰ (Wunder et al. 2006). Fertile major elemental compositions and MORB-like Sr–Nd isotopes of the low-Mg# peridotites both in Qindao and Junan regions led Ying et al. (2006) and Zhang et al. (2009b) to conclude that these low-Mg# peridotites were fragments of the newly accreted lithospheric mantle (depleted "lithospherised" asthenosphere) formed by the low-degree partial melting of asthenosphere in response to the lithospheric thinning in the late Cretaceous. The observation of the MORB-like Li isotopes in the low-Mg# lherzolite further strengthens the above conclusion.

Therefore, this study not only suggests that the low-Mg# peridotites in Jiaodong regions were the fragments of the newly accreted lithospheric mantle, but also points out that the newly accreted lithospheric mantle was almost homogeneous both in Li contents and Li isotopes. The lack of significant variation or zoning within mineral grains, which is within the analytical uncertainty, could be due to the diffusive fractionation of Li isotopes within mineral phases (Jeffcoate et al. 2007; Rudnick and Ionov 2007; Ionov and Seitz 2008).

Heterogeneity of Li contents and Li isotopes in high-Mg# harzburgites

Although the intra-mineral Li content of olivine and opx appears relatively constant, considerable variations between minerals and samples still exist in the high-Mg# harzburgites (Fig. 2; ol: 0.83–1.75 ppm; opx: 0.92–1.94 ppm). This implies that disequilibrated Li distributions between grains and samples were still preserved in these high-Mg# peridotites. Meanwhile, the presence of apparent intra- and inter-mineral variations in Li abundance of cpxs (Fig. 2; 1.12–4.89 ppm) reveals that Li

contents in these high-Mg# peridotites were far away from the equilibrium, showing a highly heterogeneous partitioning. Alternatively, this could also relate to a re-equilibration of the pyroxene at increasing pressure, which would permit the cpx to preferentially pick up labile Li during the development of jadeitic cpx via addition of Na and Li at appropriate *P–T* conditions. Moreover, similar to Hannuoba spinel lherzolites (Tang et al. 2007b), the ordering of highest Li abundance in cpx, followed by opx and with the lowest in olivine, deviates from the equilibrated Li partitioning in spinel-facies mantle (Seitz and Woodland 2000), indicating a disequilibrated Li partitioning between mineral phases and samples as well. This is further illustrated by the plot of Li in cpx vs. Li in ol (Fig. 5), in which the high-Mg# harzburgites are plotted away from the field for equilibrium partitioning of mantle xenoliths although the Li partitioning between two pyroxenes tends to be equilibrated except for PSK03-1414. The PSK03-410 with the most disequilibrium ol-cpx abundances has equilibriated cpx–opx abundances (Fig. 5). All these features imply that the Li distribution in the high-Mg# harzburgites is generally heterogeneous and that Li partitioning between pyroxenes is more liable to achieve equilibrium than that between pyroxenes and olivine, which may reflect faster diffusion of Li in pyroxenes than in olivine (Parkinson et al. 2007; Mallmann et al. 2009).

The olivine Li abundances in these high-Mg# harzburgites are similar to or even lower than the normal mantle values (Fig. 5). Such an extremely low Li concentration in olivine requires that these rocks underwent a high degree of partial melting, in agreement with the results obtained from the major elements compositions of their minerals (high Fo in olivine, high Cr# in cpx and spinel; Zhang et al. 2009b). This is also consistent with observations in the low-Mg# lherzolites that the slightly higher Li content corresponds to a lower degree of melting. Relatively higher Li abundances in opx and cpx than normal mantle values (Fig. 5) indicate that the Li enrichment in pyroxenes relative to olivine could be due to the melt/rock interaction after melting. Li abundances and variations in cpx seem correlated with other trace elements distribution (Fig. 6). Two harzburgites with high REE abundances and moderately fractionated LREE/HREE (ΣREE = 82–85 ppm, $(La/Yb)_N$ = 14–15) have a smaller range of Li contents (1.25–2.06 ppm) and a significant depletion of Li relative to other trace elements (Fig. 6). In contrast, one sample (PSK03-410) with lower REE abundance and highly fractionated LREE/HREE [ΣREE = 33 ppm, $(La/Yb)_N$ = 36] has a much wider range of Li contents (1.54–3.16 ppm) and less relative Li depletion (Fig. 6). Sample PSK03-414 which has the lowest REE abundances and limited LREE/HREE fractionation [ΣREE = 5.6 ppm, $(La/Yb)_N$ = 2.9] has a widest range of Li contents (1.12–4.89 ppm) and no Li depletion (Fig. 6). This may imply that the high-Mg# harzburgites were affected by metasomatic agents of different origins or that at least the agents were chemically heterogeneous.

In terms of Li isotopes, the overall variation of δ^7Li in olivine and opx is limited although clear Li isotope zoning exists in some grains (Fig. 2). The majorities of δ^7Li fall within the arc lava values (Moriguti and Nakamura 1998a; Tomascak et al. 2000, 2002; Chan et al. 2002a, b; Agostini et al. 2008; Košler et al. 2009) with a few beyond the MORB range, but falling in the altered MORB and peridotite xenolith fields (Fig. 3). This suggests that the high-Mg# harzburgites have the Li isotopic signature similar to the arc lavas. Although most of the previous studies have highlighted that it could not survive due to the very high diffusion rate of Li (e.g., Jeffcoate et al. 2007; Rudnick and Ionov 2007; Aulbach and Rudnick 2009; Halama et al. 2009), Vlastélic et al. (2009) argued that HIMU mantle has distinctly elevated δ^7Li and that Li isotopic heterogeneities could survive diffusion over 1–2 billion years in the mantle. Hence, we consider that the disequilibrium of Li isotopes in the mantle peridotites could be preserved for a long period (Tang et al. 2009). As a result, the arc lava-like Li isotopic compositions in the high-Mg# harzburgites indicate that these peridotites experienced metasomatism by fluids/melts possibly derived from altered MORB with variable and heavier Li isotopic compositions than the fresh MORB.

Extremely large intra-and inter-mineral variations of δ^7Li observed in cpxs (Table 1; Figs. 2, 3) demonstrate exceedingly heterogeneous δ^7Li in these high-Mg# harzburgites. A few cpxs have higher δ^7Li values, close to the values for co-existing opx and olivine (Fig. 3), showing the preservation of arc lava Li isotopic signature to a certain degree. However, the δ^7Li of the predominant cpxs are very low, with a few analyses at less than −30‰ (Table 1; Fig. 3). Low δ^7Li values have been observed in opxs of Hannuoba spinel lherzolites (Tang et al. 2007b), opxs and cpxs from Massif Central spinel lherzolites (Wagner and Deloule 2007), metasomatized peridotite and pyroxenite xenoliths (Brooker et al. 2004; Jeffcoate et al. 2007; Rudnick and Ionov 2007; Ionov and Seitz 2008; Aulbach et al. 2008; Aulbach and Rudnick 2009), eclogites (Zack et al. 2003; Marschall et al. 2007), lower crust xenoliths (Tomascak 2004; Teng et al. 2008), and Cenozoic lavas (Agostini et al. 2008), which were generally ascribed to diffusive fractionation of Li isotopes with/without rock–melt interactions or dehydration of altered oceanic crust. This Li isotope feature suggests that the high-Mg# harzburgites were affected by diffusion-driven Li isotopic fractionation during the melt/rock interaction, which will be detailed in the next section.

In summary, the high-Mg# harzburgites have substantially different characteristics in Li contents and Li isotopes

relative to the low-Mg# lherzolite, and they preserve highly heterogeneous Li contents and Li isotopes. This Li character is as expected, given that the high-Mg# peridotites are considered to be fragments of the ancient lithospheric mantle affected by the melt/rock interaction (Ying et al. 2006; Zhang et al. 2009b). Thus, our Li content and isotope results also support previous inferences that these high-Mg# peridotites were the fragments of the Archean lithospheric mantle.

Melt/rock interaction in Archean lithospheric mantle

As pointed out in the previous section, Li isotopic fractionation between mantle minerals and fluid at temperatures $> 900°C$ is $< 1.0‰$ (Wunder et al. 2006), much smaller than the differences in Li isotopic composition in our high-Mg# harzburgites. Thus, Li isotopic fractionation at high temperatures is unlikely to have produced the differences in mineral δ^7Li observed in the Qingdao high-Mg# peridotites.

Alkali elements have been reported to diffuse through silicate melts more than an order of magnitude faster than REE at high temperatures (Nakamura and Kushiro 1998; Mungall 2002). The diffusivity of alkalis in silicate melts increases with decreasing ionic radii. Li is, therefore, a fastest diffusing alkali element in silicate melts. Because the diffusion rate of ^{6}Li is faster than ^{7}Li (Richter et al. 2003), large Li isotopic fractionation can be produced by diffusion during magmatic processes (Lundstrom et al. 2005; Beck et al. 2006; Teng et al. 2006; Jeffcoate et al. 2007; Rudnick and Ionov 2007; Tang et al. 2007b). Therefore, it is possible that the large intra- and inter-mineral isotopic fractionation observed in high-Mg# peridotites were produced through Li diffusion during melt/rock interaction.

As reported in literature, light δ^7Li in cpx is due to isotope diffusive fractionation during Li ingress, probably related to the melt/rock interaction (Lundstrom et al. 2005; Jeffcoate et al. 2007; Rudnick and Ionov 2007; Tang et al. 2007b; Wagner and Deloule 2007; Aulbach et al. 2008; Aulbach and Rudnick 2009), but also may be produced during slow cooling of the xenolith in a lava (Beck et al. 2006; Ionov and Seitz 2008; Gallagher and Elliott 2009). Although the Qingdao xenoliths are hosted in lava, the Li content and Li isotopic compositions of minerals in the low-Mg# peridotite show an approximate equilibrium, indicating the small-volume lava cooled down very quickly and the Li inventories were quenched upon eruption of the host lava. So the effects of post-eruption cooling (Ionov and Seitz 2008) are probably not important in Qingdao xenoliths. Alternatively, small difference in δ^7Li between minerals in the low-Mg# peridotite may reflect Li redistribution during cooling and typically does not involve large concentration contrasts, hence being unable to produce large fractionations (Aulbach and Rudnick 2009). Therefore, the large variation in minerals of high-Mg# peridotites could be produced by diffusion-induced isotopic fractionation during peridotite–melt interaction rather than the pure effect of post-eruption cooling.

Recent modeling of diffusion-induced isotopic fractionation assumes the ingress of Li into minerals and rocks from a high Li source, such as Li diffusing into peridotite from Li-rich basaltic melt (Lundstrom et al. 2005), or into amphibolite country rocks from Li-rich pegmatite (Teng et al. 2006). In the case of Li diffusion into peridotite, the mantle minerals first became enriched in ^{6}Li because of its greater diffusion rate, resulting in a lower δ^7Li relative to its source. This diffusion mechanism was widely used to interpret the low δ^7Li in cpx of peridotite xenoliths from far-east Russia (Rudnick and Ionov 2007) and Li isotope zoning in mineral phases of peridotites from southern Siberia and Mongolia (Jeffcoate et al. 2007). The above diffusive ingress of Li may also account for the observation of isotopically heavy cores with lower Li concentrations than the light rims of minerals. Some olivine and opx grains show a similar situation like this (Fig. 2).

However, Tang et al. (2007b) found some profiles different from the above mentioned, i.e., isotopically heavy rims with lower Li abundance than the light cores in olivines and opxs, and isotopically heavy rims with higher Li abundance than the light cores in the coexisting cpxs. Generally, the partition coefficient $K_{Li}^{Ol/Cpx}$ increase with falling temperature, indicating a diffusive transfer of Li from cpx to olivine during cooling (Kaliwoda et al. 2008), which will produce Li abundance and isotopic profiles in minerals completely different from the above observed. As a result, the above observation contradicts what is expected presuming the diffusive ingress of Li into minerals as per theory (e.g., Jeffcoate et al. 2007), perhaps indicating the influence of a process other than simple diffusion. Together with the major and trace element geochemistry, they argued that the combined effects of diffusive fractionation of Li isotopes during two-stage interactions of mantle peridotites with melts originating in altered subducted oceanic crust at an earlier stage and in the asthenosphere at a later stage may be responsible for the large intra-and inter-mineral variation in Hannuoba spinel xenoliths. Wagner and Deloule (2007) found both low and high δ^7Li values at the rims of cpx and in amphiboles, suggesting a progressive ^{7}Li enrichment of the metasomatic fluid by Rayleigh distillation. The limited variation in Li concentration and Li isotopic composition within olivine and opx and an exceedingly large variation within cpxs observed in high-Mg# peridotites (Figs. 2, 3) are also difficult to interpret via only simple diffusion and require combined effects of Li diffusion during metasomatic inputs to these

harzburgites. In contrast with the variation in Li concentration and isotope ratios within minerals in Hannuoba spinel lherzolites (Fig. 3; Tang et al. 2007b), the harzburgite xenoliths in Qingdao region could have a more complicated history of melt/rock interaction:

Firstly, Li isotopes generally show a negative correlation with Li concentrations within and between samples (Fig. 4), which is the hallmark of diffusive Li isotope fractionation during Li influx.

Secondly, Li isotopes show relationships with the trace element concentrations in the samples (Fig. 6), cpxs in two harzburgites with extreme REE enrichments and moderately LREE/HREE fractionation display a smaller range in δ^7Li than the cpx grains with lower REE enrichments, in which one sample shows a clear metasomatic ingress of melt into the peridotite (Afig. 2a in electronic supplementary material). This may be related to Li diffusing faster than REE so that the effect of diffusive Li isotope fractionation will have been obscured as the heavier isotope also diffuses in, suggesting that extensive melt/rock interaction produced δ^7Li in minerals proximal to the trend of equilibrium, like the low-Mg# lherzolite does (Fig. 6). A harzburgite with moderate total REE content and an exceedingly high LREE/HREE fractionation in contrast has an extremely large range of δ^7Li (Fig. 6), showing the Li isotope fractionation induced by the metasomatic input far away from the equilibrium. Another harzburgite with lowest REE enrichment and LREE/HREE fractionation has a moderate range of δ^7Li.

Finally, large variations in Li element and δ^7Li mainly occur in the rims of minerals (Fig. 2), indicating that the mineral cores may preserve their early Li isotopic compositions. Most of the mineral cores in the harzburgites have relatively homogeneous and higher δ^7Li than the rims. These high δ^7Li values are similar to those reported for arc lavas and some altered MORB (Fig. 3). The arc lavas were generally considered to be derived from the mantle wedge metasomatized by the melts or fluids derived from the subducted oceanic slab. This indicates that the harzburgites have experienced metasomatism by agents derived from subducted materials.

Previous studies on Mesozoic mafic magmatism (Zhang et al. 2002, 2005; Zhang and Sun 2002; Ying et al. 2004; Xu et al. 2004; Fan et al. 2004; Wang et al. 2005) and mantle xenoliths (Ying et al. 2006; Zhang et al. 2009b) have shown that in the early Mesozoic the lithospheric mantle beneath the southeastern North China Craton, including the Jiaodong region, was in a similar environment to that beneath an arc. During the assembly of the Yangtze Craton into the North China Craton to form the Dabie-Sulu ultra-high metamorphic belts (Li et al. 1993), the Yangtze crustal materials were subducted underneath the lithosphere of the North China Craton. The melting of

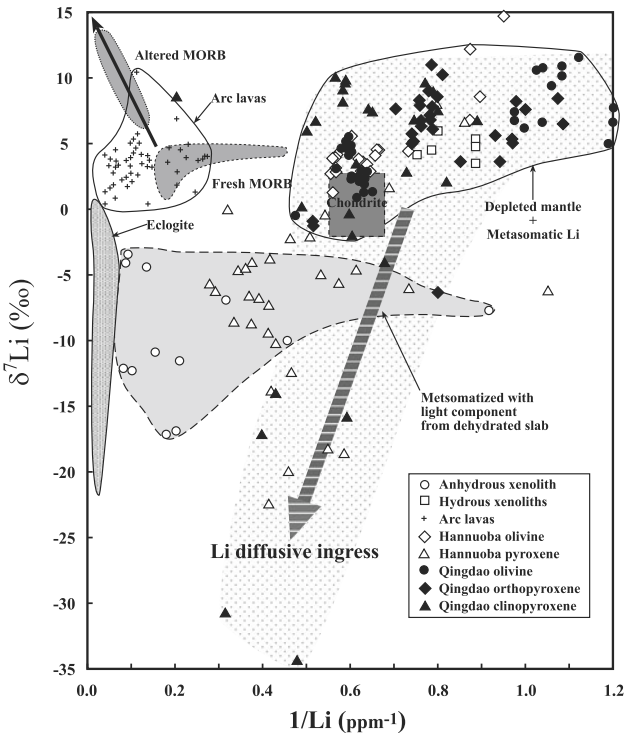

Fig. 7 Comparison of Li concentrations and isotopic ratios in high-Mg# harzburgites of this study with published data for various rock types [modified from Brooker et al. (2004) and Tang et al. (2007a)]. *Thick dash line arrow* depicts the trend of diffusive ingress of Li isotopes from melt into minerals. Data sources are identified as in Fig. 3. SIMS data of Hannuoba peridotites (Tang et al. 2007b) are included

subducted crustal materials including eclogites produced silicic melts, which migrated into the overlying lithospheric mantle and reacted with the refractory peridotite to produce Mesozoic fertile lithospheric mantle highly enriched both in trace elements and Sr–Nd isotopic compositions (Zhang et al. 2002, 2005; Zhang and Sun 2002; Ying et al. 2004; Xu et al. 2004; Fan et al. 2004; Wang et al. 2005). This process could be also responsible for the large variation in δ^7Li observed in the minerals (Fig. 7), showing the mixing trend between two endmembers: one is normal mantle peridotites with the composition close to the depleted mantle and the other is melts with variable δ^7Li derived from the subducted crustal materials. It should be noted that diffusive fractionation of Li isotopes during the peridotite–melt interactions also played an important role and could result in the extremely low δ^7Li in some cpx grains. These low δ^7Li may reflect recent ingress of Li into cpx by diffusion (e.g., Jeffcoate et al. 2007; Rudnick and Ionov 2007; Wagner and Deloule 2007; Aulbach and Rudnick 2009).

Therefore, Li abundances and Li isotopes also indicate that the Archean lithospheric mantle as represented by the high-Mg# peridotites was considerably affected by the

melt/rock interaction, consistent with the results obtained from the major and trace elemental and Sr–Nd isotopic studies.

Melt composition and origin

In the previous section, it was suggested that the Archean lithospheric mantle was considerably refertilized through the melt/rock interaction. Now the source and its composition of the melt is must be inferred. The distribution of Li between pyroxene and olivine in mineral Li–Li plots (Fig. 5) can be used to indicate melt composition in which the xenolith was affected. In a view of the Hannuoba spinel lherzolites, they plot outside the range for normal mantle (Seitz and Woodland 2000) and far from the empirical region of equilibrium partitioning of Li between pyroxene and olivine (Brenan et al. 1998). The preferential Li enrichment in pyroxene relative to olivine in these peridotites (Fig. 5), similar to the peridotite from Finero, Italy and the Hannuoba peridotites, China, which also exhibits Li enrichment in pyroxene relative to olivine, perhaps indicates that the metasomatic agent was mafic silicate melt (Seitz and Woodland 2000; Tang et al. 2007b). The Hannuoba peridotites had undergone two-stage metasomatic imprinting, i.e., early-stage metasomatic agent derived from subducted altered oceanic crust and later-stage metasomatic melt from the asthenosphere (Tang et al. 2007b). In addition, most of the peridotites from Victoria, Australia, plotting to the left side of the diagram (Fig. 5), show the influence of intrusion with carbonatitic melts, which is also consistent with the result obtained from petrological observation (Woodland et al. 2004). All these observations demonstrate that the mineral Li–Li plots of Fig. 5 can be used to deduce the melt composition. The high-Mg# harzburgites in Qingdao also plot outside the range for normal mantle (Seitz and Woodland 2000) to the right in the cpx relative to olivine, implying that these harzburgites were metasomatized by a mafic silicate melt.

The silicate melt from subducted lower crustal materials appears also to have effects on these harzburgites as evidenced by the large variations of δ^7Li in cpx and the Eu negative anomaly in sample PSK03-414 (Fig. 6), high percentage of opx in these harzburgites (Afig. 2–5 in electronic supplementary material; Zhang et al. 2009b) and enriched Sr–Nd isotopic compositions of the Mesozoic lithospheric mantle (Zhang et al. 2002). Extensive melt/rock interaction in earlier stages could homogenize the Li content and Li isotopes within samples. This may be the reason why the extremely REE-enriched samples have a narrow δ^7Li range compared to those of less REE-enriched samples (Fig. 6). This may also be the reason why the dominant minerals have δ^7Li data similar to arc lava values (Fig. 7). Fe-rich melt injection into the peridotite is also evidenced by the existence of iron spinel aggregation in PSK03-43 (Afig. 2a in electronic supplementary materiala). Thus, the Li data provide further evidence that the Archean refractory lithospheric mantle was refertilized through melt/rock interaction and transformed to the Mesozoic lithospheric mantle that was less refractory and incompatible element and Sr–Nd isotopically enriched (Zhang et al. 2002).

Conclusions

From above investigations, we can draw the following conclusions

(1) Low-Mg# lherzolite has a relatively homogeneous Li distribution and Li isotopic composition; High-Mg# harzburgites have an extremely heterogeneous Li distribution and Li isotopic compositions;
(2) This Li elemental and isotopic observation provides further evidence for the previous studies that the low-Mg# lherzolites represent the newly accreted lithospheric mantle and the high-Mg# harzburgites as fragments of refertilized Archean lithospheric mantle;
(3) Large Li elemental and isotopic disequilibria within and between minerals of Qingdao high-Mg# peridotites suggests that the Archean lithospheric mantle indeed has experienced melt/rock interaction, in which the Archean refractory lithospheric mantle was transformed to the Mesozoic less refractory one with the enrichments both in incompatible elements and Sr–Nd isotopic ratios;
(4) The cores of minerals in the high-Mg# harzburgites have relatively homogeneous δ^7Li values, which are higher than the range for MORB, but similar to those of arc lavas and some altered MORB, and indicate that the metasomatic agent had variable δ^7Li values, due to the derivation from subducted lower crustal materials. Thus, the Li data presented here provide further evidence for the existence of melt/rock interaction beneath the eastern North China Craton.

Acknowledgments Authors would like to thank X.H. Li, Y. Liu and G.Q. Tang for their assistance with Li isotope analyses in the Cameca IMS-1280 at the SIMS Lab of State Key Laboratory of Lithospheric Evolution, Institute of Geology and Geophysics, Chinese Academy of Sciences. This research was financially supported by the Nature Science Foundation of China (Grant 90714008; 40721062; 40523003) and the Chinese Academy of Sciences (Grant KZCX2-YW-103 and Bairenjihua project). Fund from the State Key Laboratory of Lithospheric Evolution is appreciated for E. Deloule's 2-week stay in Beijing, who helped us to set up the Li isotope analyses at the SIMS Lab. Horst Marschall is thanked for the suggestion on the earlier version of the manuscript. We are indebted to critical reviews and thoughtful comments by Paul Tomascak and Sonja Aulbach and the editorial suggestions of Timothy L. Grove.

References

Agostini S, Ryan JG, Tonarini S, Innocenti F (2008) Drying and dying of a subducted slab: coupled Li and B isotope variations in Western Anatolia Cenozoic Volcanism. Earth Planet Sci Lett 272:139–147

Anders E, Grevesse N (1989) Abundances of the elements: meteoritic and solar. Geochim Cosmochim Acta 53:197–214

Aulbach S, Rudnick RL (2009) Origins of non-equilibrium lithium isotope fractionation in xenolithic peridotite minerals: examples from Tanzania. Chem Geol 258:17–27

Aulbach S, Rudnick RL, McDonough WF (2008) Li-Sr-Nd isotope signatures of the plume and cratonic lithospheric mantle beneath the margin of the rifted Tanzanian craton (Labait). Contrib Mineral Petrol 155:79–92

Beck P, Chaussidon M, Barrat JA, Gillet P, Bohn M (2006) Diffusion induced Li isotopic fractionation during the cooling of magmatic rocks: the case of pyroxene phenocrysts from nakhlite meteorites. Geochim Cosmochim Acta 70:4813–4825

Bouman C, Elliott T, Vroon PZ (2004) Lithium inputs to subduction zones. Chem Geol 212:59–79

Brenan JM, Neroda E, Lundstrom CC, Shaw HF, Ryerson FJ, Phinney DL (1998) Behaviour of boron, beryllium and Lithium during melting and crystallization: constraints from mineral-melt partitioning experiments. Geochim Cosmochim Acta 62:2129–2141

Brooker RA, Jamesl RH, Blundy JD (2004) Trace elements and Li isotope systematics in Zabargad peridotites: evidence of ancient subduction processes in the Red Sea mantle. Chem Geol 212:179–204

Chan LH, Edmond JM (1988) Variations of lithium isotope composition in the marine environment: a preliminary report. Geochim Cosmochim Acta 52:1711–1717

Chan LH, Frey FA (2003) Lithium isotope geochemistry of the Hawaiian plume: results from the Hawaii Scientific Drilling Project and Koolau volcano. Geochem Geophys Geosyst 4. doi: 10.1029/2002GC000365

Chan LH, Kastner M (2000) Lithium isotopic compositions of pore fluids and sediments in the Costa Rica subduction zone: implications for fluids processes and sediments contribution to the arc volcanoes. Earth Planet Sci Lett 183:275–290

Chan LH, Edmond JM, Thompson G, Gillis K (1992) Lithium isotopic composition of submarine basalts—implications for the lithium cycle in the oceans. Earth Planet Sci Lett 108:151–160

Chan LH, Gieskes JM, You CF, Edmond JM (1994) Lithium isotope geochemistry of sediments and hydrothermal fluids of the Guaymas Basin, Gulf of California. Geochim Cosmochim Acta 58:4443–4454

Chan LH, Alt JC, Teagle DAH (2002a) Lithium and lithium isotope profiles through the upper oceanic crust: a study of seawater-basalt exchange at ODP sites 504B and 896A. Earth Planet Sci Lett 201:187–201

Chan LH, Leeman WP, You CF (2002b) Lithium isotopic composition of Central American volcanic arc lavas: implications for modification of subarc mantle by slab-derived fluids: correction. Chem Geol 182:293–300

Chan LH, Lassiter JC, Hauri EH, Hart SR, Blusztajn J (2009) Lithium isotope systematics of lavas from the Cook-Austral Islands: constraints on the origin of HIMU mantle. Earth Planet Sci Lett 277:433–442

Decitre SE, Deloule E, Reisberg L, James R, Agrinier P, Mével C (2001) Behavior of Li and its isotopes during serpentinization of oceanic peridotites. Geochem Geophys Geosyst 2:178

Fan WM, Guo F, Wang YJ, Zhang M (2004) Late Mesozoic volcanism in the northern Huaiyang tectono-magmatic belt, central China: partial melts from a lithospheric mantle with subducted continental crust relicts beneath the Dabie orogen. Chem Geol 209:27–48

Flesh GD, Anderson AR, Svec HJ (1973) A secondary isotopic standard for $^{7}Li/^{6}Li$ determination. Int J Mass Spectrom Ion Phys 12:265–272

Gallagher K, Elliott T (2009) Fractionation of lithium isotopes in magmatic systems as a natural consequence of cooling. Earth Planet Sci Lett 278:286–296

Gao S, Rudnick R, Carlson RW, McDonough WF, Liu YS (2002) Re-Os evidence for replacement of ancient mantle lithosphere beneath the North China Craton. Earth Planet Sci Lett 198:307–322

Halama R, Savov IP, Rudnick RL, McDonough WF (2009) Insights into Li and Li isotope cycling and sub-arc metasomatism from veined mantle xenoliths, Kamchatka. Contrib Mineral Petrol 158(2):197–222

Ionov DA, Seitz HM (2008) Lithium abundances and isotopic compositions in mantle xenoliths from subduction and intra-plate settings: mantle sources vs. eruption histories. Earth Planet Sci Lett 266:316–331

James RH, Rudnicki MD, Palmer MR (1999) The alkali element and boron geochemistry of the Escanaba Trough sediment-hostd hydrothermal system. Earth Planet Sci Lett 171:157–169

Jeffcoate AB, Elliott T, Kasemann SA, Ionov D, Cooper K, Brooker R (2007) Li isotope fractionation in peridotites and mafic melts. Geochim Cosmochim Acta 71:202–218

Kaliwoda M, Ludwig T, Altherr R (2008) A new SIMS study of Li, Be, B and $\delta^{7}Li$ in mantle xenoliths from Harrat Uwayrid (Saudi Arabia). Lithos 106(3–4):261–279

Košler J, Magna T, Mlcoch B, Mixa P, Nýlt D, Holub FV (2009) Combined Sr, Nd, Pb and Li isotope geochemistry of alkaline lavas from northern James Ross Island (Antarctic Peninsula) and implications for back-arc magma formation. Chem Geol 258:207–218

Li SG, Xiao YL, Liou DL, Chen YZ, Ge NJ, Zhang ZQ, Sun SS, Cong BL, Zhang RY, Hart SR, Wang SS (1993) Collision of the North China and Yangtze Blocks and formation of coesite-bearing eclogites—timing and processes. Chem Geol 109:89–111

Lundstrom CC, Chaussidon M, Hsui AT, Kelemen P, Zimmerman M (2005) Observations of Li isotopic variations in the Trinity Ophiolite: evidence for isotopic fractionation by diffusion during mantle melting. Geochim Cosmochim Acta 69:735–751

Magna T, Wiechert U, Halliday AN (2006) New constraints on the lithium isotope compositions of the Moon and terrestrial planets. Earth Planet Sci Lett 243(3–4):336–353

Mallmann G, O'Neill H, Klemme S (2009) Heterogeneous distribution of phosphorus in olivine from otherwise well-equilibrated spinel peridotite xenoliths and its implications for the mantle geochemistry of lithium. Contrib Mineral Petrol 158:485–504

Marschall HR, Pogge von Strandmann PAE, Seitz HM, Elliott T, Niu Y (2007) The lithium isotopic composition of orogenic eclogites and deep subducted slabs. Earth Planet Sci Lett 262:563–580

Menzies M, Xu YG, Zhang HF, Fan WM (2007) Integration of geology, geophysics and geochemistry: a key to understanding the North China Craton. Lithos 96:1–21

Moriguti T, Nakamura E (1998a) Across-arc variation of Li isotopes in lavas and implications for crust/mantle recycling at subduction zones. Earth Planet Sci Lett 163:167–174

Moriguti T, Nakamura E (1998b) High-yield lithium separation and the precise isotopic analysis for natural rock and aqueous samples. Chem Geol 145:91–104

Mungall JE (2002) Empirical models relating viscosity and tracer diffusion in magmatic silicate melts. Geochim Cosmochim Acta 66:125–143

Nakamura E, Kushiro I (1998) Trace element diffusion in jadeite and diopside melts at high pressures and its geochemical implication. Geochim Cosmochim Acta 62:3151–3160

Nishio Y, Nakai S, Yamamoto J, Sumino H, Matsumoto T, Prikhod'ko VS, Arai S (2004) Lithium isotopic systematics of the mantle-derived ultramafic xenoliths: implications for EM1 origin. Earth Planet Sci Lett 217:245–261

Ottolini L, Laporte D, Raffone N, Devidal JL, Le FB (2009) New experimental determination of Li and B partition coefficients during upper mantle partial melting. Contrib Mineral Petrol 157:313–325

Parkinson IJ, Hammond SJ, James RH, Rogers NW (2007) High-temperature lithium isotope fractionation: insights from lithium isotope diffusion in magmatic systems. Earth Planet Sci Lett 257:609–621

Richter FM, Davis AM, Depaolo DJ, Watson EB (2003) Isotope fractionation by chemical diffusion between molten basalts and rhyolite. Geochim Cosmochim Acta 67:3905–3923

Rudnick RL, Ionov DA (2007) Lithium elemental and isotopic disequilibrium in minerals from peridotite xenoliths from far-east Russia: product of recent melt/fluid-rock reaction. Earth Planet Sci Lett 256:278–293

Seitz HM, Woodland AB (2000) The distribution of lithium in peridotitic and pyroxenitic mantle lithologies—an indicator of magmatic and metasomatic processes. Chem Geol 166:47–64

Seitz HM, Brey GP, Lahaye Y, Durali S, Weyer S (2004) Lithium isotopic signatures of peridotite xenoliths and isotopic fractionation at high temperature between olivine and pyroxenes. Chem Geol 212:163–177

Tang YJ, Zhang HF, Ying JF (2007a) Review of the lithium isotope systems as a geochemical tracer. Int Geol Rev 49:274–388

Tang YJ, Zhang HF, Nakamura E, Moriguti T, Kobayashi K, Ying JF (2007b) Lithium isotopic systematics of peridotite xenoliths from Hannuoba, North China Craton: implications for melt/rock interaction in the considerably thinned lithospheric mantle. Geochim Cosmochim Acta 71:4327–4341

Tang YJ, Moriguti T, Zhang HF, Nakamura E, Tanaka R, Kobayashi K, Ying JF (2009) Li–Sr–Nd isotopic disequilibrium between minerals of peridotite xenoliths from the North China Craton: evidence for multistage melt–peridotite interactions in the refertilized lithospheric mantle. Geochim Cosmochim Acta (in press)

Teng FZ, McDonough WF, Rudnick RL, Dalpé C, Tomascak PB, Chappell BW, Gao S (2004) Lithium isotopic composition and concentration of the upper continental crust. Geochim Cosmochim Acta 68:4167–4178

Teng FZ, McDonough WF, Rudnick RL, Walker RJ (2006) Diffusion-driven extreme lithium isotopic fractionation in country rocks of the Tin Mountain pegmatite. Earth Planet Sci Lett 243:701–710

Teng FZ, Rudnick RL, McDonough WF, Gao S, Tomascak PB, Liu YS (2008) Lithium isotopic composition and concentration of the deep continental crust. Chem Geol 255:47–59

Tomascak PB (2004) Developments in the understanding and application of lithium isotopes in the Earth and planetary sciences. In: Johnson CM, Beard BI, Albarede F (eds) Geochemistry of non-traditional stable isotope: reviews in mineralogy and geochemistry, vol 55. Mineral Society of America, Washington DC, pp 153–195

Tomascak PB, Tera F, Helz R, Walker RJ (1999) The absence of lithium isotope fractionation during basalt differentiation: new measurements by multicollector sector ICP-MS. Geochim Cosmochim Acta 63:907–910

Tomascak PB, Ryan JG, Defant MJ (2000) Lithium isotope evidence for light element decoupling in the Panama sub-arc mantle. Geology 28:507–510

Tomascak PB, Widom E, Benton LD, Goldstein SL, Ryan JG (2002) The control of lithium budgets in island arcs. Earth Planet Sci Lett 196:227–238

Tomascak PB, Langmuir CH, le Roux PJ, Shirey SB (2008) Lithium isotopes in global mid-ocean ridge basalts. Geochim Cosmochim Acta 72:1626–1637

Vlastélic I, Koga K, Chauvel C, Jacques G, Télouk P (2009) Survival of lithium isotopic heterogeneities in the mantle supported by HIMU-lavas from Rurutu Island, Austral Chain. Earth Planet Sci Lett 286:456–466

Wagner C, Deloule E (2007) Behaviour of Li and its isotopes during metasomatism of French Massif Central lherzolites. Geochem Cosmochem Acta 71:4279–4296

Wang YJ, Fan WM, Peng TP, Zhang HF, Guo F (2005) Nature of the Mesozoic lithospheric mantle and tectonic decoupling beneath the Dabie Orogen, Central China: evidence from $^{40}Ar/^{39}Ar$ geochronology, elemental and Sr–Nd–Pb isotopic compositions of early Cretaceous mafic rocks. Chem Geol 220:165–189

Woodland AB, Seitz HM, Yaxley GM (2004) Varying behaviour of Li in metasomatised spinel peridotite xenoliths from western Victoria, Australia. Lithos 75:55–66

Wu FY, Walker RJ, Yang YH, Yuan HL, Yang JH (2006) The chemical-temporal evolution of lithospheric mantle underlying the North China Craton. Geochim Cosmochim Acta 70:5013–5034

Wunder B, Meixner A, Romer RL, Heinrich W (2006) Temperature-dependent isotopic fractionation of lithium between clinopyroxene and high-pressure hydrous fluids. Contrib Mineral Petrol 151:112–120

Xu YG, Ma JL, Huang XL, Iizuka Y, Chung SL, Wang YB, Wu XY (2004) Early Cretaceous gabbroic complex from Yinan, Shandong Province: petrogenesis and mantle domains beneath the North China Craton. Int J Earth Sci 93:1025–1041

Ying JF, Zhou XH, Zhang HF (2004) Geochemical and isotopic investigation of the Laiwu-Zibo carbonatites from western Shandong Province, China and implications for their petrogenesis and enriched mantle source. Lithos 75:413–426

Ying JF, Zhang HF, Kita N, Morishita Y, Shimoda G (2006) Nature and evolution of Late Cretaceous lithospheric mantle beneath the eastern North China Craton: constraints from petrology and geochemistry of peridotitic xenoliths from Junan, Shandong province, China. Earth Planet Sci Lett 244:622–638

You CF, Chan LH (1996) Precise determination of lithium isotopic composition in low concentration natural samples. Geochim Cosmochim Acta 60:909–915

Zack T, Tomascak PB, Rudnick RL, Dalpé C, McDonough WF (2003) Extremely light Li in orogenic eclogites: the role of isotope fractionation during dehydration in subducted oceanic crust. Earth Planet Sci Lett 208:279–290

Zhang HF, Sun M (2002) Geochemistry of Mesozoic basalts and mafic dikes in southeastern North China Craton and tectonic implication. Int Geol Rev 44:370–382

Zhang L, Chan LH, Gieskes JM (1998) Lithium isotope geochemistry of pore waters, Ocean Drilling Program Sites 918 and 919, Irminger Basin. Geochim Cosmochim Acta 62:2437–2450

Zhang HF, Sun M, Zhou XH, Fan WM, Zhai MG, Yin JF (2002) Mesozoic lithosphere destruction beneath the North China Craton: evidence from major, trace element, and Sr-Nd-Pb isotope studies of Fangcheng basalts. Contrib Mineral Petrol 144:241–253

Zhang HF, Sun M, Zhou XH, Ying JF (2005) Geochemical constraints on the origin of Mesozoic alkaline intrusive complexes from the North China Craton and tectonic implications. Lithos 81:297–317

Zhang HF, Goldstein SL, Zhou XH, Sun M, Zheng JP, Cai Y (2008a) Evolution of subcontinental lithospheric mantle beneath eastern

China: Re–Os isotopic evidence from mantle xenoliths in Paleozoic kimberlites and Mesozoic basalts. Contrib Minerol Petrol 155:271–293

Zhang J, Zhang HF, Ying JF, Tang YJ, Niu LF (2008b) Contribution of subducted Pacific slab to Late Cretaceous mafic magmatism in Qingdao region, China: a petrological record. Island Arc 17(2):231–241

Zhang HF, Goldstein SL, Zhou XH, Sun M, Cai Y (2009a) Comprehensive refertilization of lithospheric mantle beneath the North China Craton: further Os–Sr–Nd isotopic constraints. J Geol Soc London 166:249–259

Zhang J, Zhang HF, Kita N, Shimoda G, Morishita Y, Ying JF (2009b) Secular evolution of the lithospheric mantle beneath eastern North China Craton: evidence from peridotitic xenoliths from Late Cretaceous mafic rocks in Jiaodong region, China. Int Geol Rev. doi:10.1080/00206810903025090